PALEOCEANOGRAPHY, VOL. 28, 607–618, doi:10.1002/palo.20047, 2013

Changes in the advection of Antarctic Intermediate Water to the northern Chilean coast during the last 970 kyr

G. Martínez-Méndez,[1] D. Hebbeln,[1] M. Mohtadi,[1] F. Lamy,[2] R. De Pol-Holz,[3] D. Reyes-Macaya,[3] and T. Freudenthal[1]

Received 8 February 2013; revised 13 August 2013; accepted 16 August 2013; published 1 October 2013.

[1] The Antarctic Intermediate Water (AAIW) is a key player in global-scale oceanic overturning processes and an important conduit for heat, fresh water, and carbon transport. The AAIW past variability is poorly understood mainly due to the lack of sedimentary archives at intermediate water depths. We present records of benthic stable isotopes from sediments retrieved with the seafloor drill rig MARUM-MeBo at 956 m water depth off northern Chile (GeoB15016, 27°29.48′S, 71°07.58′W) that extend back to 970 ka. The sediments at this site are presently deposited at the boundary between AAIW and Pacific Deep Water (PDW). For previous peak interglacials, our results reveal similar benthic $\delta^{13}C$ values at site GeoB15016 and of a newly generated stack of benthic $\delta^{13}C$ from various deep Pacific cores representing the "average PDW." This suggests, unlike today, the absence of AAIW at the site and the presence of nearly pure PDW. In contrast, more positive $\delta^{13}C$ values at site GeoB15016 compared to the stack imply a considerable AAIW contribution during cold phases of interglacials and especially during glacials. Besides, we used three short sediment cores to reconstruct benthic $\delta^{13}C$ values from the AAIW core during the last glacial and found a $\delta^{13}C$ signature similar to today's. Assuming that this was the case also for the past 970 kyr, we demonstrate that sea level changes and latitudinal migrations of the AAIW formation site can only account for about 50% of the full range of past $\delta^{13}C$ increases at site GeoB15016 during cold periods. Other processes that could explain the remaining of the positive $\delta^{13}C$ anomalies are increases in glacial AAIW production and/or deeper convection of the AAIW with respect to preceding interglacials.

Citation: Martínez-Méndez, G., D. Hebbeln, M. Mohtadi, F. Lamy, R. De Pol-Holz, D. Reyes-Macaya, and T. Freudenthal (2013), Changes in the advection of Antarctic Intermediate Water to the northern Chilean coast during the last 970 kyr, *Paleoceanography*, *28*, 607–618, doi:10.1002/palo.20047.

1. Introduction

[2] In the last decades, the conceptual view of past climatic changes being mainly driven by North Atlantic climatology is supplemented by the recognition that Southern Hemisphere processes are also active players in global climate change and ocean reorganizations. An important water mass forming in the Southern Ocean is the Antarctic Intermediate Water (AAIW) that contributes to the ventilation of waters of the subtropical gyres [*Sijp and England*, 2009; *Sloyan and Rintoul*, 2001] and participates in the global distribution of heat, fresh water, and carbon [e.g., *Fischer et al*., 2010; *Talley*, 1999]. Furthermore, it is the main constituent of the so-called "cold water route" of the return flow that compensates for the export of the North Atlantic Deep Water (NADW) to the world oceans [*Rintoul*, 1991; *Sloyan and Rintoul*, 2001]. The AAIW appears as one of the main oceanic sinks for the present-day, anthropogenic-forced excess atmospheric CO_2 [*Sabine et al*., 2004; *Sallee et al*., 2012]. It is suggested that the AAIW was also tightly connected with the carbon cycle and atmospheric CO_2 variations in the past [e.g., *Anderson et al*., 2009; *Basak et al*., 2010; *Marchitto et al*., 2007] whereas the evidence are not unequivocal [*De Pol-Holz et al*., 2010; *Rose et al*., 2010; *Sortor and Lund*, 2011]. Moreover, it has been argued that the AAIW played a key role in past ocean rapid reorganizations [*Pahnke and Zahn*, 2005; *Pahnke et al*., 2008; *Saenko et al*., 2003].

[3] Despite the importance of this water mass, not much is known about its long-term development mainly due to the scarcity of long sedimentary records from the AAIW water depths (typically 500 to 1200 m). To date, only one paleoceanographic study exists from such a depth range (core MD97-2120) that reaches beyond the last glacial period [*Pahnke and Zahn*, 2005]. Core MD97-2120 was recovered

Additional supporting information may be found in the online version of this article.

[1]MARUM-Center for Marine Environmental Sciences, University of Bremen, Bremen, Germany.
[2]Alfred Wegener Institute for Polar and Marine Research, Bremerhaven, Germany.
[3]Department of Oceanography and Center for Climate and Resilience Research, Universidad de Concepción, Concepción, Chile.

Corresponding author: G. Martínez-Méndez, MARUM-Center for Marine Environmental Sciences, University of Bremen, Leobener Strasse, DE-28359 Bremen, Germany. (gmartinez@marum.de)

0883-8305/13/10.1002/palo.20047

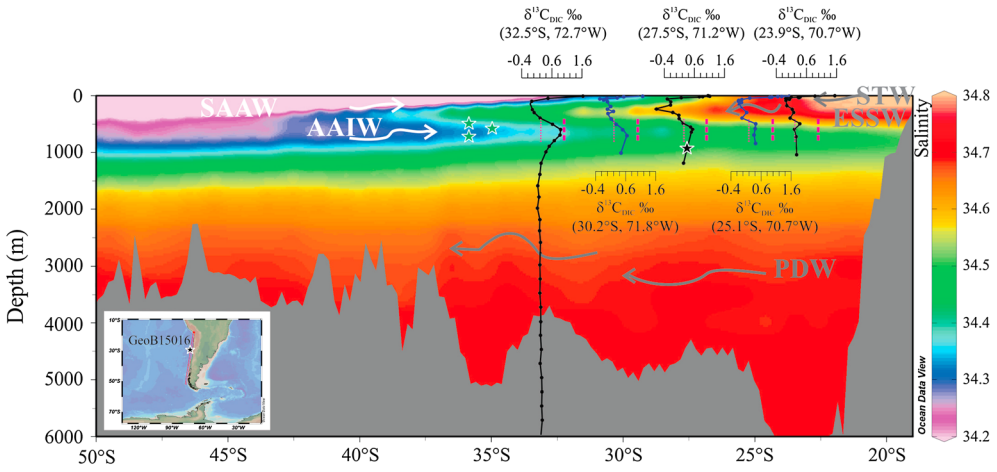

Figure 1. Location of Site GeoB15016 (black star) at the Chilean margin (see inset) and within a longitudinal salinity transect (data from the World Ocean Atlas 2009, mean annual salinity [*Antonov et al.*, 2010]) through the SE Pacific (along the red line in inset) indicating the regional distribution of main water masses (maps are compiled with the software ODV [*Schlitzer*, 2012]). These are the northward flowing, low salinity Subantarctic Surface Water (SAAW) and Antarctic Intermediate Water (AAIW) and the more saline, southward flowing Subtropical Water (STW), Equatorial Subsurface Water (ESSW), and Pacific Deep Water (PDW). In addition to low salinities, the AAIW is further indicated by high $\delta^{13}C_{DIC}$ values as shown by vertical distributions of $\delta^{13}C_{DIC}$ in the water column at stations along the Chilean margin. From south to north, these stations are WOCE Station P06E-011 (32.5°S, 72.7°W [*Kumamoto et al.*, 2011]), GeoB15024 (30.2°S, 71.8°W), GeoB15004 (27.5°S, 71.2°W), GeoB15007 (25.1°S, 70.7°), and GeoB15011 (23.9°S, 70.7°W). For orientation, the stippled red lines indicate $\delta^{13}C_{DIC}$ values of 0.2‰ (thin line) and 1‰ (bold line), respectively. The green stars indicate the location of the short gravity cores used to reconstruct the $\delta^{13}C$ signature of the AAIW during the last glacial period.

from the Chatham Rise (Southwest (SW) Pacific) and provides evidence of a bipolar seesaw in the convection of the AAIW and NADW for the last three glacial-interglacial cycles (last 345 kyr) with increased production of the AAIW corresponding to Southern Hemisphere warming periods [*Pahnke and Zahn*, 2005]. During the Last Glacial Maximum (LGM), an increased AAIW production has not been detected off New Zealand [*Pahnke and Zahn*, 2005], whereas in the Tasman Sea, a thickening in the ocean layer occupied by this water mass was inferred [*Bostock et al.*, 2004]. Additionally, other proxy and model studies suggest increased LGM production of this water mass elsewhere [*Herguera et al.*, 2010; *Muratli et al.*, 2010; *Wainer et al.*, 2012]. This study fills the knowledge gap regarding the long-term variability of the AAIW by presenting a long benthic stable isotope record from the Southeast (SE) Pacific, an area sensitive to AAIW variability, which extends back to 970 ka. We moreover present water column $\delta^{13}C_{DIC}$ measurements, which we use to unravel the potential mechanisms of change in the advection of the AAIW in this region.

2. Regional Setting

[4] The Chilean margin at ~27.5°S is characterized by five main water masses, which comprise from surface to the ocean floor the Subtropical Water (STW), Subantarctic Water (SAAW), Equatorial Subsurface Water (ESSW), Antarctic Intermediate Water (AAIW), and Pacific Deep Water (PDW) [e.g., *Silva et al.*, 2009, and references therein] (Figure 1). The STW is advected by the Peru-Chile Counter Current (PCCC) and flows poleward in the upper 50 m of the water column close to the Chilean coast. Its thickness increases farther offshore and at 100°W it can be identified down to ~200 m [*Silva et al.*, 2009]. The SAAW originates from the Southern Ocean and is transported equatorward at the surface by the Peru-Chile Current (PCC) (or Humboldt Current (HC)) [e.g., *Llanillo et al.*, 2012; *Schneider et al.*, 2007]. At around 35°S, the core of this cold, fresh water mass can sink below the STW [*Silva et al.*, 2009]; however, it can also stay at the surface farther to the north by displacing the STW offshore [e.g., *Llanillo et al.*, 2012]. Below SAAW/STW, the ESSW, associated with the Oxygen Minimum Zone (OMZ) of the SE Pacific Ocean, flows poleward driven by the Poleward Undercurrent (PU) (or Gunther Undercurrent (GUC)) [e.g., *Leth et al.*, 2004]. Close to the coast at 28°S, the ESSW covers the depth range from around 100 to 400 m water depth, overlying the AAIW that has a measurable contribution of 30–40% down to ~1000 m [e.g., *Silva et al.*, 2009; *Llanillo et al.*, 2012]. Nearby its formation regions (with the main one off southern Chile, e.g., *Hanawa and Talley* [2001]), the depth range of the core of the AAIW is 600 to 1300 m [*Dickson et al.*, 2001; *Sloyan and Rintoul*, 2001]. The thickness of the AAIW is progressively decreased toward the North and its core slightly shoals (400 to 1000 m). Underneath the AAIW, southward flowing PDW fills the basin [*Leth et al.*, 2004; *Shaffer et al.*, 2004].

[5] The carbon isotopic composition of the dissolved inorganic carbon ($\delta^{13}C_{DIC}$) of the AAIW and the PDW is of relevance for the present study. *Bostock et al.* [2013] define a positive range of 0.6–1.7‰ for the AAIW that is formed in the SE Pacific, the main formation region of the AAIW today. In combination with $\delta^{13}C$ values from WOCE line P19

[*Talley*, 2005] stretching latitudinally along ~87°W, a mean $\delta^{13}C_{DIC}$ value of 1.25‰ can be considered as representative for the AAIW in the SE Pacific (see Figure S1 in Text S1 in the supporting information). In contrast, PDW, the most abundant water in the world's oceans, is characterized by much lower $\delta^{13}C_{DIC}$ values. A $\delta^{13}C_{DIC}$ value of 0‰ accounts for the majority of the volume of this water mass, although due to the lack of convection of deep water in the Pacific today, its $\delta^{13}C_{DIC}$ progressively decreases toward the north from typical values of Circumpolar Deep Water (~0.5‰) in the South Pacific to values as low as −0.5‰ in the North Pacific [*Kroopnick*, 1985]. At WOCE station P06E-011 (32.5°S, 72.72°W), $\delta^{13}C_{DIC}$ from 1200 to 6000 m water depth fluctuates around 0.2‰ [*Kumamoto et al*., 2011] indicating the presence of an atypical PDW south of site GeoB15016.

3. Materials and Methods

3.1. Core Material

[6] This study is based on long sedimentary records obtained with the MARUM-MeBo deep-sea drill rig [*Freudenthal and Wefer*, 2007; *Freudenthal and Wefer*, 2009] from the Chilean margin. Two parallel holes were drilled during the R/V *Sonne* expedition ChiMeBo (SO-211) in November 2010 at site GeoB15016 off northern Chile (27°29.48′S, 71°07.58′W) at 956 m water depth. The two holes, GeoB15016-1 and GeoB15016-2, were separated by only 20 m at the same location. GeoB15016-1 and GeoB15016-2 reached drilling depths of 56.75 and 57.35 m below seafloor (mbsf) with recoveries of 87% and 75%, respectively. In addition, the 207 cm long gravity core GeoB15005-1 was retrieved from the same position. Today, site GeoB15016 lies at the boundary between the AAIW and the PDW (see Figure 1).

3.2. Composite Record of Site GeoB15016

[7] In order to obtain a sedimentary sequence as continuous as possible, a composite record of the two cores was generated following the Integrated Ocean Drilling Program procedures. The splicing method consisted of a series of iterative steps using onboard color scan data, shore-based X-ray fluorescence (XRF) scan measurements and benthic stable isotope data. A preliminary composite was generated based on visual correlation of color scan data measured on board in the two cores. A subsequent refinement of the composite was done with XRF core scanner data (obtained with an AVAATECH XRF Scanner at MARUM, University of Bremen, Germany; for a detailed methodical description see *Röhl and Abrams* [2000]). The 2 cm resolved elemental counts data were used for a detailed hole-to-hole correlation. We mainly used the log(Fe/Ca) record but crosschecked with records of the other measured elements (see Figures S2-1 to S2-5 in Text S2 in the supporting information). The new composite record reached 58.67 m composite depth (mcd). Gaps in the sedimentary sequence were identified where sediment recovery in one of both holes was poor and therefore no matching of the XRF records was possible. For none of the records, stretching or expansion procedures were applied. The depths (mcd) with the best visual fit in the records of the two cores were chosen for the splicing (these are indicated in Figures S2-1 to S2-5). Subsequently, samples were taken every 10 cm along the composite. In those sections where the XRF and color data were not showing clear similarities and it was therefore not possible to conclusively define matching sections, samples from both cores were taken. For all these samples, stable isotope measurements on benthic foraminifera were performed (see section 3.3.) and used to corroborate and/or redefine the existing composite. The identified gaps from the XRF data were corroborated by the $\delta^{18}O$ stratigraphy as the sections above and below the gap were easily correlated to the benthic $\delta^{18}O$ stack of *Lisiecki and Raymo* [2005] (referred to as LR04; see section 4.2. for age model development).

[8] Further details of the splicing and resulting composite record are shown in Text S2. The first drilling interval from 0 to 2.70 mbsf resulted in low sediment recovery in both cores (35 and 105 cm). Therefore, for the upper part of the composite record we used the gravity core GeoB15005-1 (207 cm long) from the same location, which unfortunately was still not long enough to reach the second drilling interval of either GeoB15016-1 or GeoB15016-2 (Figure 2).

[9] The final composite record of 58.67 mcd contains six gaps: between 2.07 mcd and 3.02 mcd (i.e., between 33 and 82 ka, see below for details on the age model), between 23.48 and 23.91 mcd (i.e., between 452 and 457 ka), between 30.82 and 30.92 mcd (548–549 ka), between 45.4 and 47.47 mcd (742–779 ka), between 52.11 and 52.34 mcd (845–848 ka), and between 54.71 and 55.17 mcd (883–891 ka). The gaps comprise less than 7% of the total record. In comparison to the maximum drilling depth (57.35 mbsf), the composite depth of nearly 59 mcd indicates approximately 3.5% of sediment expansion.

3.3. Stable Isotope Measurements

[10] To prepare oxygen ($\delta^{18}O$) and carbon ($\delta^{13}C$) isotope measurements on benthic foraminifera, the composite record of GeoB15016 was sampled at an average of 10 cm intervals. The 2 cm thick samples were freeze-dried and washed over a 63 µm sieve. On average, three to four individuals of benthic foraminifera were handpicked from the 355–425 µm size fraction.

[11] An initial screening of samples distributed along the core showed that *Fontbotia wuellerstorfi* (also commonly referred to as *Cibicidoides* or *Planulina*) was not always present downcore. Instead, *Cibicidoides kullenbergi* (or *C. mundulus*) appeared present in most of the samples also displaying better preservation. *F. wuellerstorfi* is the preferred species in paleoceanographic studies because its test incorporates $\delta^{13}C$ in equilibrium with the ambient water and hence, allows for the reconstruction of deep-sea $\delta^{13}C$ in the past [e.g., *Curry et al*., 1988; *Duplessy et al*., 1988; *Zahn et al*., 1986]. Also, *C. kullenbergi* is frequently used for this purpose [e.g., *Flower and Kennett*, 1995; *Holbourn et al*., 2004; *Keigwin*, 1987], although it is shown that sometimes *C. kullenbergi* may record lower $\delta^{13}C$ values than those of ambient water suggesting an occasional infaunal habitat [*Hodell et al*., 2001]. Thus, a continuous record on *C. kullenbergi* was established and wherever possible, complemented by measurements on *F. wuellerstorfi* in order to correct for potential offsets in the isotopic composition between *F. wuellerstorfi* and *C. kullenbergi*. In total, 417 samples of *C. kullenbergi* and 167 of *F. wuellerstorfi* were measured, from which 114 are paired measurements of the two species (Figure 2).

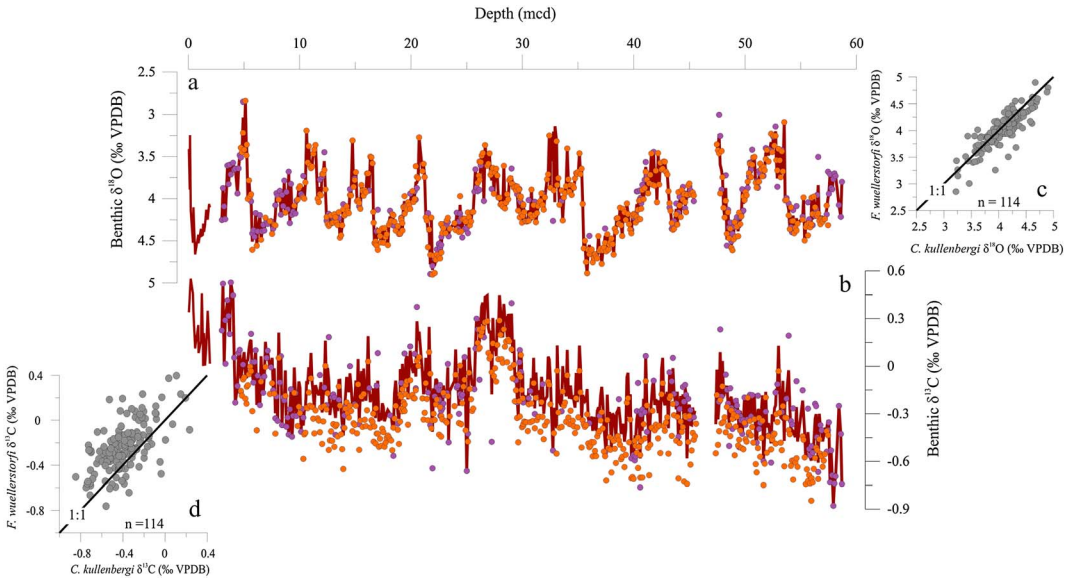

Figure 2. Stable isotope records of GeoB15016 in the composite depth scale (meters composite depth, mcd). (a) Combined stable oxygen isotope ($\delta^{18}O$) record of *C. kullenbergi* and *F. wuellerstorfi* in brown. (b) Combined stable carbon isotope ($\delta^{13}C$) record of *C. kullenbergi* (corrected by 0.16‰, see text) and *F. wuellerstorfi* in brown. For both records, the individual original values of *C. kullenbergi* are displayed in orange and of *F. wuellerstorfi* in purple. Double measurements of both species on the same samples displayed in the insert plots illustrate the relationship between the $\delta^{18}O$ data of both species approximating a 1:1 line and between the $\delta^{13}C$ data revealing an offset between both species (see text).

[12] The gravity core GeoB15005-1 was sampled at varying intervals of 4 to 28 cm. For this core, mixed species of *Cibicidoides* were used for the stable isotope analyses.

[13] Stable carbon isotopes of *F. wuellerstorfi* and *Cibicidoides* spp. in samples from the last glacial period (Marine isotope stage (MIS) 2) were also measured in gravity cores GeoB3359-3 (35°13′S, 72°48′W, 678 m water depth; see *Romero et al.* [2006] for age model), GeoB7163-7 (36°26′S, 73°36′W, 537 m water depth; *De* Pol-Holz et al., unpublished age model, 2012) and GeoB7165-1 (36°33′S, 73° 40′W, 797 m water depth; see *Mohtadi et al.* [2008] for age model).

[14] All stable oxygen and carbon isotopes were measured with a Thermo Finnigan MAT 252 mass spectrometer linked online to a single acid bath CarboKiel-II carbonate preparation device at the MARUM isotope laboratory. Analytical standard deviation was monitored through the internal laboratory standard Solnhofen Limestone (SHK) and was 0.05‰ VPDB for $\delta^{13}C$ and 0.07‰ VPDB for $\delta^{18}O$. Isotope values were calibrated to the Vienna Peedee Belemnite scale with the NBS 19 standard.

3.4. Water Samples

[15] Water samples for measuring the $\delta^{13}C_{DIC}$ were collected from different water depths at four stations during the expedition SO-211 (Figure 1 and Table 1) using Niskin bottles. Part of the water collected in Niskin bottles was siphoned into 100 mL glass bottles avoiding bubbles and with enough water to fill the bottles twice. The samples were poisoned with 50 µL of $HgCl_2$ to prevent biological modification of the actual $\delta^{13}C_{DIC}$ composition and sealed with wax. The samples were kept at 4°C until measuring at the MARUM isotope laboratory in Bremen. Measurements were carried out in a gas bench coupled to a Thermo Finnigan MAT 252 mass spectrometer using 1 mL of seawater. The long-term standard deviation based on routine measurements of the internal standard SHK was better than 0.1‰. The internal standard was calibrated against NBS 19 and seawater from the deep Atlantic Ocean.

4. Results

4.1. Estimating Potential Isotopic Offsets Between *F. wuellerstorfi* and *C. kullenbergi*

[16] Paired measurements (n = 114) of *F. wuellerstorfi* and *C. kullenbergi* revealed that there is no offset between the $\delta^{18}O$ values of the two species as $\delta^{18}O_{wuell}$-$\delta^{18}O_{kull} = -0.06‰ \pm 0.17$ (1σ), i.e., the difference is close to the analytical error of 0.07‰. An ANOVA (analyses of variance) two-way test with the null hypothesis also shows that there is no difference between the $\delta^{18}O$ of the two species at a confidence level of 95%. Subsequently, the results of $\delta^{18}O$ of the two species were combined. In order to do so, for samples with paired measurements, the mean between the $\delta^{18}O$ values obtained for the two species was computed and included in the record (Figure 2).

Table 1. Water Sample Stations Along the Northern Chilean Margin

Station name	Latitude (S)	Longitude (W)	Maximum Water Depth (m)
GeoB15004-1	27°26.66′	71°08.92′	1197
GeoB15007-1	25°03.56′	70°39.56′	923
GeoB15011-1	23°51.15′	70°38.75′	1106
GeoB15024-1	30°14.08′	71°46.64′	1098

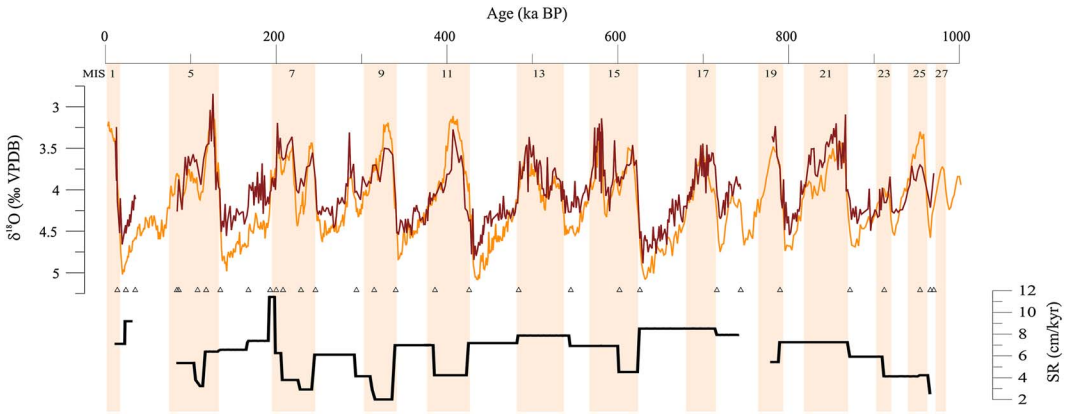

Figure 3. Age model for site GeoB15016. The age model was derived by linking the benthic $\delta^{18}O$ records (brown) of MeBo core GeoB15016 and of the gravity core GeoB15005-1 (corresponding to the period from 33 to 8 ka) to the LR04 global benthic $\delta^{18}O$ stack of *Lisiecki and Raymo* [2005] (orange). Gaps in the site GeoB15016 $\delta^{18}O$ record indicate intervals missing due to reduced sediment recovery in the respective sections. White triangles indicate the tie points used for the correlation of this site to the LR04 stack. The resulting sedimentation rates (SR in cm/kyr) for site GeoB15016 are illustrated by the bold black line. Vertical shading highlights interglacial Marine Isotope Stages (MIS) indicated at the top.

[17] In contrast, the $\delta^{13}C$ values of *C. kullenbergi* were depleted compared to those of *F. wuellerstorfi* (Figure 2). The mean difference between the $\delta^{13}C$ values of *F. wuellerstorfi* and *C. kullenbergi* resulting from the 114 paired samples amounts to 0.16‰ ± 0.16 (1σ) and also an ANOVA two-way test at the 95% confident interval corroborates that significant differences exist between the $\delta^{13}C$ values of the two species. A second ANOVA two-way test confirms the null hypothesis that the difference in $\delta^{13}C$ between the two species is 0.16‰ and consequently, the *C. kullenbergi* $\delta^{13}C$ values were corrected by adding 0.16‰ to match the *F. wuellerstorfi* signal and, thus, the $\delta^{13}C$ of the ambient bottom waters. *Hodell et al.* [2003] observed that in glacial sections of South Atlantic cores, $\delta^{13}C$ values of *C. kullenbergi* tend to be lower than of *F. wuellerstorfi*, whereas in interglacial sections the offset disappears. We did not observe any glacial-interglacial pattern in the $\delta^{13}C$ offset between the two species.

4.2. Age Model

[18] The age model for the sediment record at site GeoB15016 (including the gravity core GeoB15005-1 for the youngest part of the record) was developed by graphical correlation of the benthic $\delta^{18}O$ record to the LR04 benthic $\delta^{18}O$ stack of *Lisiecki and Raymo* [2005] (see Table S1 in Text S3 for tie points between GeoB15016 and LR04). The GeoB15016 $\delta^{18}O$ record shows orbital modulation with obvious glacial-interglacial variability that covers the period from MIS 26 to MIS 5, from approximately 970 to 80 ka with only some minor gaps (Figure 3). Gravity core GeoB15005-1 covers the period from 33 to 8 ka. The GeoB15016 $\delta^{18}O$ record generally displays lower values than the LR04 stack [*Lisiecki and Raymo*, 2005], particularly during glacial periods. Because of these lower values in glacial periods, the glacial-interglacial transitions were smaller in GeoB15016 compared to the LR04 stack.

[19] The sedimentation rates at site GeoB15016 varied between 2 and 11 cm/kyr with a mean value of 7 cm/kyr. Generally, lower (higher) sedimentation rates occurred during peak interglacial (glacial) periods. The average 10 cm sampling step in GeoB15016 resulted in a temporal resolution between 0.76 and 9.62 kyr with a mean value of 1.63 kyr.

4.3. Benthic Foraminiferal Carbon Isotope Record

[20] The GeoB15016 $\delta^{13}C$ record shows glacial-interglacial modulation with on average 0.2–0.4‰ higher values during interglacial than during glacial periods. Only between MIS 13 and 14 the glacial-interglacial amplitude is ~0.5‰. Early Holocene $\delta^{13}C$ values at the site range from ~0.34 to 0.44‰, which is in good agreement with a reported value of $\delta^{13}C_{DIC}$ of 0.4‰ at 990 m depth in the nearby WOCE station P06E-011 [*Kumamoto et al.*, 2011], and with an estimated value of 0.4‰ (see below) at 956 m depth at station GeoB15004-1 that is only three nautical miles away from site GeoB15016. Such high values have only been recorded at the end of MIS 5 (from ca 116 to 80 ka) and during MIS 13. However, for the most of the last 970 kyr, the $\delta^{13}C$ values remained below 0‰. Most depleted average values are observed for the oldest sections of the core with values reaching −0.9‰ during MIS 25.

4.4. Changes in $\delta^{13}C$ and $\delta^{18}O$ of the PDW Over the Last 1 Myr

[21] In order to analyze changes in the contribution of the PDW and AAIW to site GeoB15016, we generated stacks of $\delta^{13}C$ and $\delta^{18}O$ signatures of the PDW (PDW_{stack}) covering the last 1 Myr. We adopted the procedure by *Lisiecki* [2010] who produced a $\delta^{13}C$ PDW stack for the past 800 kyr using records from ODP sites 849, 846, 677, and 806. For this study, a new 1 Myr PDW_{stack} was required that ideally represents the purest possible PDW end-member nearby the Chile Basin. Therefore, ODP site 806 was removed from *Lisiecki*'s [2010] database because it is located on the Ontong Java Plateau in the western equatorial Pacific at comparably shallow depths (2520 m). Besides, Site 806 only covers the last 730 kyr whereas ODP sites 849, 846, and 677

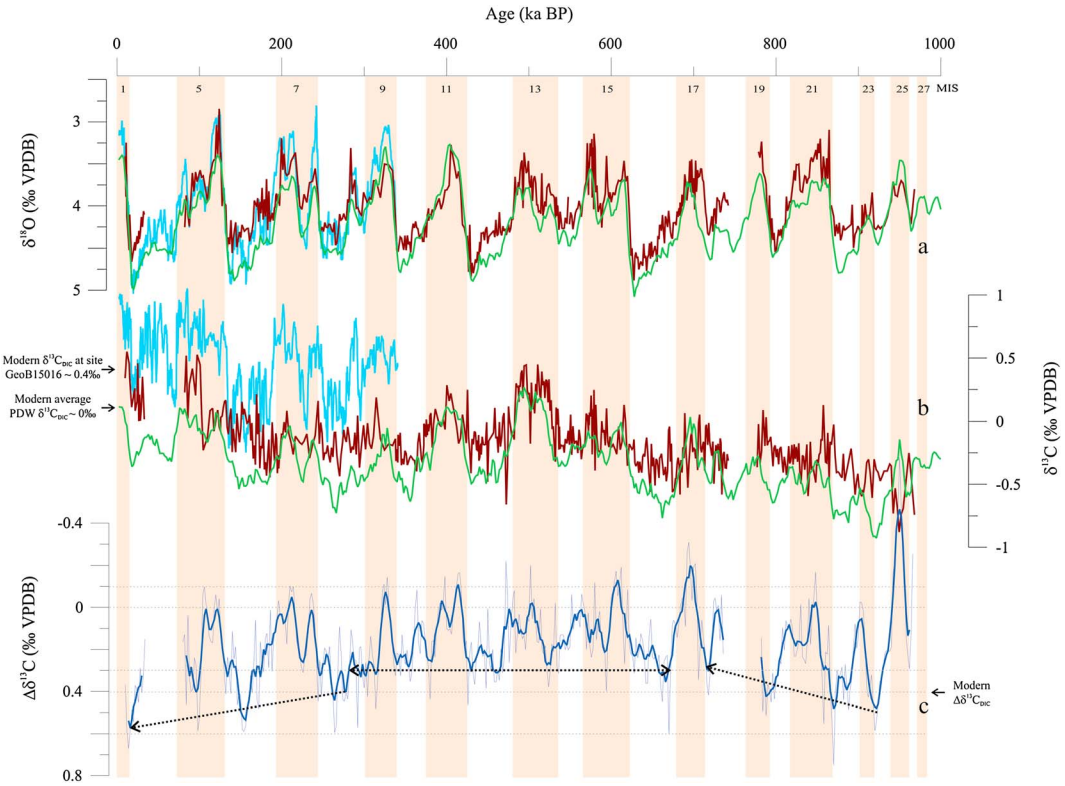

Figure 4. Stable isotope ($\delta^{18}O$ and $\delta^{13}C$) records from the Pacific. (a) Benthic $\delta^{18}O$ records of GeoB15016 (brown), of the new PDW_{stack} (green, see text), and of MD97-2120 from the SW Pacific (light blue, a five-point running mean of the original data set is displayed for clarity) [*Pahnke and Zahn*, 2005]. (b) Benthic $\delta^{13}C$ records of GeoB15016 (brown), of the new PDW_{stack} (green), and of MD97-2120 from the SW Pacific (light blue, a five-point running mean of the original data set is displayed for clarity) [*Pahnke and Zahn*, 2005]. (c) The $\delta^{13}C$ gradient between GeoB15016 and the PDW stack ($\Delta\delta^{13}C$). Thick line shows a five-point running mean over the record. The modern values for the water column $\delta^{13}C_{DIC}$ at site GeoB15016 and the average present value for PDW are shown in Figure 4b. Also in Figure 4c, the present $\Delta\delta^{13}C$ (modern $\delta^{13}C_{DIC}$ at site GeoB15016 - 0‰ for modern PDW, see text) for site GeoB15016 is indicated. Vertical shading highlights interglacial Marine Isotope Stages (MIS) indicated at the top.

reach beyond 1.3 Ma. The original stable isotope records and further details on the stack are shown in Text S4.

[22] The newly generated PDW_{stack} provides insight into the variability of the $\delta^{13}C$ and $\delta^{18}O$ values of the PDW during the last 1 Myr (Figure 4) with the $\delta^{18}O$ PDW_{stack} largely following the global LR04 stack [*Lisiecki and Raymo*, 2005] (see Figure S4-1 in Text S4). The $\delta^{13}C$ PDW_{stack} displays lower glacial than interglacial values with glacial-interglacial amplitudes varying from 0.36‰ between MIS 20 and 19 to 0.7‰ between MIS 10 and 9.

4.5. Intermediate to Deep Water $\delta^{13}C$ Gradient Over the Last 1 Myr

[23] The $\delta^{13}C$ PDW_{stack} has been subtracted from the GeoB15016 record ($\Delta\delta^{13}C_{GeoB15016\text{-}PDW}$) in order to remove the deep Pacific component from the local record and to better assess the AAIW contribution at 956 m water depth off subtropical Chile for the last 970 kyr (see discussion). To do so, the GeoB15016 record was rescaled at a 2 kyr pacing to match the resolution of the PDW_{stack} (see Figure S4-2). By subtracting these two records from each other all mean ocean $\delta^{13}C$ changes [e.g., *Duplessy et al*., 1988] originating from changes in the global carbon cycle, and global trends in the $\delta^{13}C$ [e.g., *Hoogakker et al*., 2006] are removed from the $\Delta\delta^{13}C_{GeoB15016\text{-}PDW}$ record. Thus, the $\Delta\delta^{13}C_{GeoB15016\text{-}PDW}$ record reflects "true" site-specific variations in the $\delta^{13}C$ signal, which are driven by changing contributions of PDW and AAIW to the site (Figure 4c).

[24] The $\Delta\delta^{13}C_{GeoB15016\text{-}PDW}$ record fluctuates between −0.2 and +0.6‰ (an extreme negative value of ca −0.5‰ during MIS 25 is not considered) with values close to zero or slightly negative during peak interglacials and positive values during cold interglacial and glacial periods. Three sections can be identified in this record: (i) from 970 to 720 ka, where the glacial $\Delta\delta^{13}C_{GeoB15016\text{-}PDW}$ seems to become progressively smaller, while a gap in the sedimentary sequence in MIS 18 makes it difficult to firmly identify a trend; (ii) between circa 720 and 280 ka, the glacial increases in the $\Delta\delta^{13}C_{GeoB15016\text{-}PDW}$ are of the same order; and (iii) from 280 to 16 ka, when the glacial $\Delta\delta^{13}C_{GeoB15016\text{-}PDW}$ positive anomalies increase.

4.6. Carbon Isotope Distribution in the Water Column

[25] Vertical profiles of $\delta^{13}C_{DIC}$ down to intermediate depths were measured at four stations off northern Chile. These data are presented together with data from station

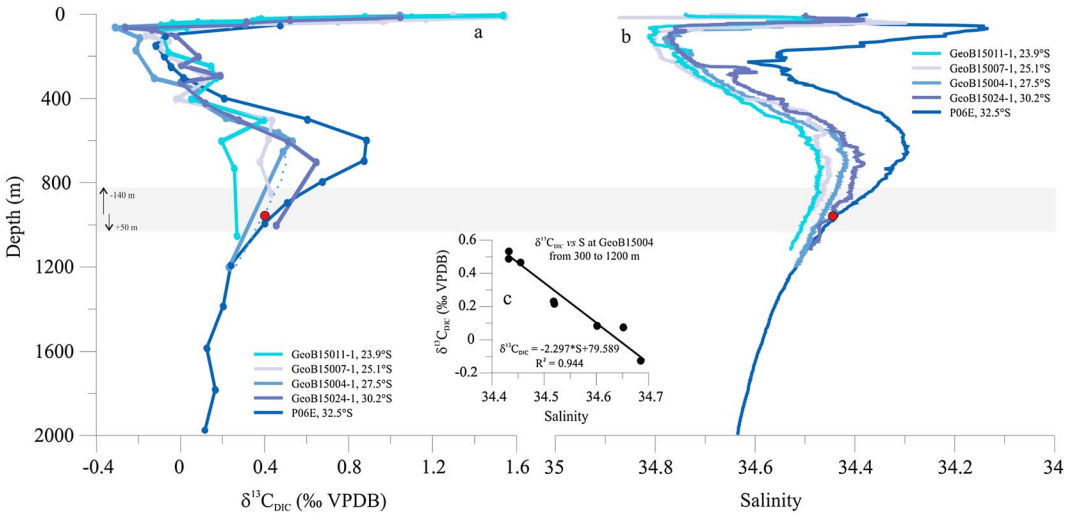

Figure 5. Vertical water column profiles of (a) $\delta^{13}C_{DIC}$ and (b) salinity (b) at various latitudes along the Chilean margin (P06E-11 $\delta^{13}C_{DIC}$ and S data are from *Kumamoto et al*. [2011]). (c) Inset figure illustrates the relationship between $\delta^{13}C_{DIC}$ and salinity at station GeoB15004-1 (i.e., site GeoB15016), thus justifying the use of the high-resolution salinity profiles to calculate the detailed vertical $\delta^{13}C_{DIC}$ distribution between 600 and 1200 m at this site, and the bottom water value of 0.4‰ at the coring location in 956 m depth (red dot in Figure 5a). The dotted line indicates the most likely trend of decrease of $\delta^{13}C_{DIC}$ following the salinity trend (red dot in Figure 5b indicates the site position in the salinity profile). The grey shading illustrates the maximum range of sea level variability over the last 970 ka according to *Elderfield et al*. [2012] in relation to site GeoB15016 (red dot).

P06E-011 (32.5°S, 72.72°W) [*Kumamoto et al*., 2011] in Figures 1 and 5. The $\delta^{13}C_{DIC}$ values were high at the surface and rapidly decreased to values between −0.2 and 0‰ from approximately 60 to 200 m water depth at all four stations. From 200 to 400 m water depth (depth range of the ESSW), the values were slightly positive fluctuating between 0 and 0.2‰. Between 400 and 900 m water depth, the $\delta^{13}C_{DIC}$ values were more positive as characteristic for the AAIW. The $\delta^{13}C_{DIC}$ maxima of 0.4, 0.44, 0.51, and 0.65‰ at each station (from north to south) were measured at 500, 500, 600, and 700 m water depth. These values are depleted respect to the 0.9‰ value measured at 600 and 700 m at station P06E-11 [*Kumamoto et al*., 2011]. The data show a clear latitudinal trend at intermediate depths with progressively more positive values toward the southern stations. At station GeoB15024-1, significantly more positive $\delta^{13}C_{DIC}$ values (0.45‰) are observed at 1000 m water depth while at the northernmost station, $\delta^{13}C_{DIC}$ reached values of only 0.3–0.2‰ at the same depth (Figures 1 and 5). Close to site GeoB15016, station GeoB15004-1 reveals the most positive value of 0.5‰ at 600 m water depth with values decreasing to 0.2‰ at 1200 m. Applying the covariance of the salinity profiles and the $\delta^{13}C_{DIC}$ profiles at this station (and also at station P06E-11; Figure 5) [*Kumamoto et al*., 2011] that show a very good linear relationship (Figure 5c), a $\delta^{13}C_{DIC}$ value of 0.4‰ was interpolated for 956 m water depth, where core GeoB15016 was retrieved.

5. Discussion

[26] The AAIW is an important component of the global ocean circulation yet its past variability is poorly understood. The main formation area of this water mass today is in the SE Pacific, off southern Chile [e.g., *Hanawa and Talley*, 2001]. The core of the AAIW is clearly identified by minimum salinity and positive $\delta^{13}C_{DIC}$ values (Figures 1 and 5). The initial depth range close to the formation site is 600–1300 m [*Sloyan and Rintoul*, 2001] and becomes progressively narrowed as the AAIW spreads northward with the type properties becoming eroded by mixing with the surrounding water masses. Site GeoB15016 lies at the northward reaches of the AAIW along the Chilean margin and at its lower boundary with the PDW. The benthic $\delta^{13}C$ record at intermediate depths off Chile registers past shifts in the proportion of the PDW and the AAIW, changes in the isotopic signature of either water mass, or a combination of both.

5.1. Reliability of Shell $\delta^{13}C$ Values of Benthic Foraminifera as a Water Mass Tracer

[27] The $\delta^{13}C$ of *F. wuellerstorfi* and related taxa (e.g., *Cibicidoides* species) may be lowered under high productivity conditions [*Mackensen et al*., 1993]. The formation of a fluffy layer of organic matter at the ocean floor may generate a microenvironment of low $\delta^{13}C$ prone to be recorded by the foraminifera [*Mackensen et al*., 1993]. Consequently, in such a case the foraminifera do not faithfully record the bottom water $\delta^{13}C$ signal.

[28] The coastal region off Chile is one of the most productive regions of the world oceans [e.g., *Berger et al*., 1987]. However, for core GeoB3388-1 retrieved ~270 nm offshore from site GeoB15016 and well within the reach of nutrient-rich filaments of upwelling waters, productivity effects on the benthic $\delta^{13}C$ signal have been discarded for the past 1 Myr [*Mohtadi et al*., 2006]. This assessment is based on the covariance of the $\delta^{13}C$ records of benthic and planktonic foraminifera within this core. Increased surface productivity and subsequent increased export of organic matter would generate $\delta^{13}C$ signals of opposite sign in the planktonic and

benthic foraminiferal records which is not observed in core GeoB3388-1 [*Mohtadi et al*., 2006]. In light of the comparable environmental setting of both cores, we conclude that productivity effects did not alter the benthic foraminiferal $\delta^{13}C$ signature at site GeoB15016.

[29] Additionally, *F. wuellerstorfi* $\delta^{13}C$ measurements in core-top samples distributed along the Chilean margin under different productivity conditions were in good agreement with $\delta^{13}C$ values of ambient waters (M. Marchant et al., unpublished data, 2006), therefore, further supporting the reliability of the benthic $\delta^{13}C$ record of GeoB15016 to trace water mass variability today and thus in the past.

5.2. AAIW Variability on the Chilean Slope at 27.5°S

[30] During most interglacial periods, the $\delta^{13}C$ and $\delta^{18}O$ values of GeoB15016 and the PDW_{stack} are very similar (Figures 4a and 4b). This similarity suggests the presence of nearly pure PDW at this site during past warm periods. In contrast, during glacial periods, almost continuously more positive $\delta^{13}C$ values at GeoB15016 compared to the PDW_{stack} indicate a measurable glacial presence of AAIW at the site, which is the only regional water mass carrying a notably more positive $\delta^{13}C$ signal today and most likely also in the past (see below for further discussion) (Figure 4b). This conclusion is supported by the comparison of the $\delta^{18}O$ record of GeoB15016 with the $\delta^{18}O$ record of the PDW_{stack} (Figure 4a), which reveals very similar values for the interglacials and more depleted values in the GeoB15016 record during glacial periods of the last 970 kyr. These (glacial) depletions can be linked to warmer AAIW temperatures compared to those of the PDW that controls the $\delta^{18}O$ PDW_{stack} signal. Interestingly, for the end of MIS 5 and for the earliest Holocene a substantial offset between both $\delta^{13}C$ records suggests a significantly stronger influence of the AAIW at 956 m water depth off northern Chile as compared to earlier interglacials.

[31] The $\Delta\delta^{13}C_{GeoB15016\text{-}PDW}$ highlights the observations extracted by visual comparison of the $\delta^{13}C$ records. During peak interglacials from MIS 23 to MIS 5e, the $\Delta\delta^{13}C_{GeoB15016\text{-}PDW}$ was close to zero or even slightly negative indicating the (almost) exclusive presence of PDW at the sampling site. Such a hydrographic configuration with essentially zero contribution of AAIW to this site during past peak interglacial periods was radically different from the present—peak interglacial—situation, in which water column $\delta^{13}C$ (and T-S) data clearly reveal a distinct offset from typical PDW values (Figures 1 and 5) thereby indicating the presence of the AAIW. In contrast, evident increases in the $\Delta\delta^{13}C_{GeoB15016\text{-}PDW}$ of on average 0.4 ± 0.1‰, as found along the shift from most interglacials into the subsequent glacial period and between peak interglacial and cold phases of interglacial periods, point to a substantial AAIW contribution to the local bottom waters at site GeoB15016 (Figure 4c) during colder times. Enhanced glacial presence of the AAIW at site GeoB15016 appears in agreement with other reconstructions applying redox-sensitive proxies and benthic $\delta^{13}C$, as well as modeling studies [*Herguera et al*., 2010; *Muratli et al*., 2010; *Wainer et al*., 2012]. These studies suggest an increased production of the AAIW during the LGM.

[32] Thus, the PDW was likely the sole contributor to intermediate water flow at ~1000 m depth at 27.5°S off Chile during peak interglacials of the last 970 kyr whereas during cold interglacial phases (e.g., MIS 5a-d, 7d, 9a, 11a) and during glacial periods the AAIW reached this location.

5.3. Mechanisms Contributing to Observed Changes in the Regional Water Column Structure

[33] Assuming that in the past AAIW and PDW were, as today, the main water masses at site GeoB15016, there are several mechanisms that could alter the amount of the AAIW at our location: (i) changes in the preformed isotopic signature of the AAIW, when a more $\delta^{13}C$-enriched glacial-AAIW would contribute to the offset with the PDW_{stack} record; (ii) sea level changes, i.e., sea level lowering (rising) would move the core of the AAIW closer to (apart from) site GeoB15016; (iii) circum-Antarctic frontal movements, when assumed glacial northward migrations of the fronts would have displaced the AAIW formation site equatorward, hence allowing for a further northward penetration of this water mass; and (iv) a possible fourth (active) mechanism invokes increases/decreases in the production of AAIW. In the following, we discuss each of these possible mechanisms in detail:

[34] (i). So far, there is no long published record within the core of the AAIW comprising glacial sediments (i.e., deposited under a lowered sea level) in the SE Pacific. The benthic $\delta^{13}C$ record of *Pahnke and Zahn* [2005] at the lower boundary of the AAIW in the SW Pacific suggests that the AAIW maintained a very positive $\delta^{13}C$ signature during at least the last 345 kyr as it displays almost continuously positive $\delta^{13}C$ values (when mean ocean changes in $\delta^{13}C$ are taken into account). This record is shown in Figure 4 for reference. Our data from the SE Pacific also suggest that the AAIW maintained a rather positive $\delta^{13}C$ signature in this region. For the AAIW to maintain a positive $\delta^{13}C$ during past times, the formation should have occurred in contact with the atmosphere, i.e., in a sea ice-free region, similarly to today. Besides, colder glacial temperatures have the potential to generate a more positive $\delta^{13}C$ glacial-AAIW due to enhance fractionation during CO_2 exchange at cold temperatures [*Mook et al*., 1974; *Charles et al*., 1993] theoretically further aided by stronger winds during glacials (e.g., see *Kohfeld et al*. [2013] for a review). A glacial cooling of 5–10°C could increase the $\delta^{13}C$ of seawater by 0.1–0.5‰ [*Mook et al*., 1974; *Charles et al*., 1993]. *Ho et al*. [2012] reported lower glacial sea surface temperatures by 6-8 °C from sediment cores off Southern South America for the past 700 kyr, which could indicate the degree of glacial cooling in the vicinity of the convection site of the AAIW. Thus, this effect may not be negligible. Nonetheless, if the formation site of the AAIW shifted northward together with equatorward migrations of the circum-Antarctic fronts (i.e., displacement toward warmer latitudes), the northward location of the convection site could partially compensate for the glacial cooling effect on the $\delta^{13}C$. With all, genuine changes in the isotopic signature of the AAIW in past times may play a role in the variations we observed off northern Chile, whereas the degree of this effect is impossible to determinate without a long record within the core of the AAIW in the SE Pacific.

[35] To assess changes in the AAIW $\delta^{13}C$ composition in a glacial period, we measured benthic foraminifera $\delta^{13}C$ values in samples of the last glacial period (MIS 2) taken from a set of short sediment cores collected within the present-day core

of the SE Pacific AAIW along the Chilean margin (GeoB3359-3, GeoB7163-7, GeoB7165-1; see Figure 1 and methods for depth and location). The benthic foraminiferal $\delta^{13}C$ values ranged between 0.4 and 0.64‰, i.e., close to 1‰ when accounted for a mean ocean depletion of 0.32‰ during the last glacial [*Duplessy et al*., 1988]. Thus, the AAIW in the SE Pacific had a $\delta^{13}C$ signature similar to that of today during the last glacial period, suggesting that a northward migration of the formation site indeed compensated the glacial cooling effect on $\delta^{13}C$ fractionation upon formation. We assume that also in previous times the AAIW maintained a $\delta^{13}C$ similar to today's, and therefore our interpretations of increase presence of this water mass to site GeoB15016 during cold periods would be produced by mechanisms ii to iv.

[36] (ii). Sea level lowering during glacial times has the potential to place the core of the AAIW closer to site GeoB15016. We use $\delta^{13}C_{DIC}$ values of the present-day water column to evaluate the rate of change of this property with depth (Figures 1 and 5).

[37] The present-day $\delta^{13}C_{DIC}$ profile of WOCE station P06E-11 (32.5°S, 72.7°W) reveals the strongest AAIW signal (0.9‰) at ~600–700 m and a not yet typical PDW signal of 0.2‰ from ~1400 to 6000 m water depth [*Kumamoto et al*., 2011]. Thus, along the transition zone between both water masses, i.e., between 700 and 1400 m, the average gradient can be set to ~0.1‰ per 100 m. The same exercise can be done for station GeoB15004-1 (27.5°S, 71.2°W, close to site GeoB15016), where the gradient between an eroded AAIW signature at 650 m water depth ($\delta^{13}C_{DIC} = 0.49$‰) and the deepest measurement at this station (1200 m, $\delta^{13}C_{DIC} = 0.23$‰) amounts to only 0.035‰/100 m. The estimates indicate on one hand that this rate varies with latitude and on the other hand that it is rather small, particularly at the northern station where the type characteristics of the AAIW are already altered. Assuming an average glacial-interglacial sea level variability of ~100–120 m [e.g., *Elderfield et al*., 2012], the resulting sea level effect in the $\delta^{13}C_{DIC}$ signature at the depth of the core would be in the order of +0.1‰ at 32.5°S and of +0.04‰ at 27.5°S, too small to account for the observed offset of $\Delta\delta^{13}C_{GeoB15016\text{-}PDW}$ during past cold periods.

[38] (iii). Today the formation mechanisms of the AAIW are still disputed between two main schools, one suggesting that the formation in the SE Pacific occurs mainly by isopycnal exchange at the Polar Front (PF) [e.g., *Molinelli*, 1981] and the other indicating convection by winter cooling of Subantarctic Mode Water (SAMW) north of the Subantarctic Front [e.g., *McCartney*, 1977; *Talley*, 1999]. Either way, frontal movements across the past 970 kyr may have shifted the formation site of AAIW northward/southward hence influencing the northward spreading of this water mass to site GeoB15016 without changes in the vigor of its formation. Most studies dealing with latitudinal migrations of the circum-Antarctic Fronts conclude either northward migrations during glacials of up to 5–9° (e.g., *Becquey and Gersonde* [2003] in the Atlantic; *Caniupán et al.* [2011], *Hebbeln et al*. [2007], and *Ho et al.* [2012] in the SE Pacific) or no movement (e.g., *Schäfer et al*. [2005] off New Zealand) with topographic constraints potentially explaining the lacking of movements recorded off New Zealand [e.g., *Hayward et al*., 2012].

[39] Presently, the $\delta^{13}C_{DIC}$ maxima of 0.9‰ at 600 and 700 m water depth at station P06E-11 associated with the AAIW were progressively eroded and displaced to shallower depths with the northward advance of this water mass with values as low as 0.4‰ and 0.3‰ in the two northernmost stations (GeoB15007-1, 25.1°S and GeoB15011-1, 23.9°S). At 600 m water depth, from station P06E-11 to station GeoB15004-1, the $\delta^{13}C_{DIC}$ decreases by nearly 0.4‰ over 5° of latitude, whereas at 800 m water depth the decrease is only 0.2‰. At 1000 and 1200 water depth there is virtually no change in $\delta^{13}C_{DIC}$ between these two stations. Therefore, the water column $\delta^{13}C_{DIC}$ profiles indicate that the positive $\delta^{13}C$ signature diagnostic of the AAIW is more rapidly eroded at the core of the water mass (~600–700 m) than at the upper or lower boundaries. Considering this observation, it is worthy to evaluate the potential effects of a latitudinal migration of the formation site of the AAIW together with variations in the rate of change at depth.

[40] Table 2 allows estimating the combined effects of sea level lowering and northward movement of the fronts on the water column $\delta^{13}C_{DIC}$ signal following the above mentioned considerations. Assuming that the AAIW $\delta^{13}C$ signature was similar to today's in the past (based on our limited assessment for MIS 2), for peak glacial periods with boundary conditions in the range of ~100–120 m lower sea level and a conservative estimate of a northward frontal displacement by ~5° [e.g., *Gersonde et al*., 2005], the resulting change in $\delta^{13}C$ should be equivalent to an increase of $\delta^{13}C$ from presently ~0.4‰ at station GeoB15004-1 (~site GeoB15016) to ~0.6‰ as the estimated value at 856–836 m water depth at P06E-11. Thus, the combined effect of glacial sea level lowering and northward frontal movements on the $\delta^{13}C$ signal at site GeoB15016 amounts to an increase on the order of ~0.2‰. In contrast, an interglacial with a higher sea level (up to ~50 m, e.g., MIS 11 [*Elderfield et al*., 2012]) and a hypothesized more southward location of the fronts compared to the present day could decrease the $\delta^{13}C$ by ~0.13‰ (from ~0.4‰ at 950 m water depth at station GeoB15004-1 to 0.27–0.26‰ at 1000 m water depth at station GeoB15011-1).

[41] For most glacial inceptions, our generated $\Delta\delta^{13}C$ increases however by ~0.4‰; therefore, some additional mechanism should be involved to explain the remaining ~0.2‰ glacial $\delta^{13}C$ increase at site GeoB15016. Some studies suggest an increase in the production of the AAIW during the LGM [*Herguera et al*., 2010; *Muratli et al*., 2010; *Wainer et al*., 2012] and this could lead to a stronger presence of this water mass at site GeoB15016. Thus, we cautiously suggest that (iv) an increased production rate of AAIW during all glacial periods of the past 970 kyr may have contributed the remaining (or part of) 0.2‰ of the observed glacial $\Delta\delta^{13}C$ increase of 0.4‰. Alternatively, or in addition to an increased production, the depth of convection of the AAIW may have been deeper during glacials [e.g., *Bostock et al*., 2004; *Keeling and Stephens*, 2001; *Wainer et al*., 2012], which also would have resulted in higher $\delta^{13}C$ values at our site. We cannot assess that possibility with the existing data sets and therefore our inference about past changes in productive remains speculative.

[42] Some periods throughout the last 1 Ma are marked by larger glacial-interglacial differences in the $\Delta\delta^{13}C$ signal (MIS 23/22: ~0.5‰; MIS 17/16: ~0.6‰; MIS 9/8: ~0.5‰,

Table 2. $\delta^{13}C_{DIC}$ Water Column Profiles Off Chile[a]

Depth (m)	P06E-11 (32.5°S, 72.7°W)	GeoB15024-1 (30.2°S, 71.8°W)	GeoB15004-1 (27.5°S, 71.2°W)	GeoB15007-1 (25.1°S, 70.7°W)	GeoB15011-1 (23.9°S, 70.7°W)
~600	0.9	0.5	0.53	0.4	0.2
~700	0.87	0.65	*~0.52*	0.38	0.26
800	0.7		*~0.49*	0.43	
836	***~0.6***		*~0.48*		
856	***~0.6***		*~0.46*		
900	0.51		*~0.44*		
956	*~0.44*		***~0.41***		
1000	0.4	0.45	*~0.38*		***~0.26***
1050					0.27
~1200	0.24		0.23		

[a]The values in italics are not real measurements but linearly interpolated values using S versus $\delta^{13}C_{DIC}$ correlations. The values in bold indicate values at 27.5°S at the depth of site GeoB15016 and possible positions of the site when glacial-interglacial sea level variations and frontal movements are considered, i.e., glacial sea level lower by 100–120 m and northward frontal movement of ~5° (shifting to 32.5°S), higher interglacial sea level by 50 m and southward frontal movement by ~4° (shifting to 23.9°S).

MIS 7/6: ~0.6‰, MIS 5/2: ~0.6‰) (Figure 4c). As sea level lowering was not larger than 100–120 m for those periods [*Elderfield et al*., 2012], and larger frontal movements with a postulated concomitant displacement of the formation site of the AAIW may have not been involved, more vigorous AAIW production or deeper convection may account for the higher $\Delta\delta^{13}C$ values during these intervals.

[43] Likewise, during MIS 2, the $\Delta\delta^{13}C$ is large (~0.6‰) indicating a high presence of AAIW. For MIS 2, we were able to estimate $\delta^{13}C$ values within the core of the AAIW (which were similar to present ones); thus, for this period we can confidently use the present water column $\delta^{13}C_{DIC}$ distribution to emulate glacial boundary conditions. In fact, a northward frontal shift of 5° [*Gersonde et al*., 2005] and a 100 m lower sea level [*Elderfield et al*., 2012] appear sufficient to explain the difference between the LGM and modern data (Table 2). This finding does not align with the conclusions of *Muratli et al*. [2010] who investigated redox-sensitive proxies in intermediate-depth ODP sites from around 41°S–36°S at the Chilean margin. They concluded either an increased LGM production of the AAIW or a better oxygenation of this water mass (or a combination of both) in the SE Pacific compared to the Holocene, during which their redox-sensitive proxies show hardly any variability [*Muratli et al*., 2010]. Since older interglacials show quite some variability in the AAIW advection (see Figure 4), the *Muratli et al*. [2010] records might indeed be more sensitive to oxygenation than to AAIW production changes. The MIS 2 $\Delta\delta^{13}C$ is nonetheless the largest of the entire record so in absolute terms this was the period with the strongest presence of AAIW at site GeoB15016.

[44] Another intriguing finding in our data set is the potential of an existing seesaw in the production of the AAIW between the SE and SW Pacific. The SW Pacific data of the last 345 kyr by *Pahnke and Zahn* [2005] were interpreted to reflect increased production of the AAIW during warm periods, i.e., interglacial times and warm glacial phases linked to Antarctic warming, and decreased production during cold glacial phases. Our data from the SE Pacific point toward a reverse situation with evidence of weaker presence of AAIW, maybe related to decreased production, during warm periods and increase presence, maybe partly caused by increased production, in cold stages. Increased glacial production can be explained by increased Ekman transport as a result of more intense glacial winds and higher densities [*Wainer et al*., 2012] and/or enhanced winter sea ice formation with denser and deeper glacial-AAIW that formed seasonally at the sea ice edge [*Keeling and Stephens*, 2001]. The dichotomy between the SE and SW Pacific emphasizes the necessity of regional considerations when analyzing the variability of the AAIW. Four types of AAIW are defined today in the Pacific [*Bostock et al*., 2013] and the differences between the different AAIW types could have been larger in the past [*Makou et al*., 2010]. Larger differences between various glacial-AAIWs could be related to different formation processes that are not yet understood, and which may have important implications for the global ocean circulation.

[45] The present-day situation with a significant presence of the AAIW at site GeoB15016 appears exceptional when compared with other peak interglacials. Unfortunately, our Holocene $\delta^{13}C$ record does not allow determining whether the advection of the AAIW to site GeoB15016 during the Holocene climatic optimum might have been weaker, similarly to older peak interglacials. The present-day hydrographical configuration with larger advection of the AAIW to the northern coast of Chile appeared to start in MIS 5d, when an abrupt $\delta^{13}C$ increase of ~0.4‰ in our GeoB15016 record (and not recorded in the PDW_{stack}) is observed at the transition from MIS 5d to 5c. The high $\delta^{13}C$ values last at least until the end of MIS 5. With maximum sea level variations of 40 m [*Elderfield et al*., 2012] and probably without any larger latitudinal migrations of the fronts during this period, the resulting strong positive $\Delta\delta^{13}C$ signal may suggest a change in the oceanographical conditions toward a stronger presence of the AAIW since then, including the LGM.

[46] Alternatively, the modern situation might be a snapshot within a peak interglacial indicating strong short-term variability (possibly decadal to centennial) in the production of the AAIW, as indicated by the observations of a decreasing production and changes in the properties of the AAIW within the past decades [*Wong et al*., 1999; *Schmidtko and Johnson*, 2012].

6. Conclusions

[47] We present the so far longest benthic stable isotope records from intermediate depths in the SE Pacific, an area sensitive to AAIW variability. The records from 956 m water

depth off northern Chile (27.5°S) extend back to 970 ka. Comparison of the benthic stable carbon isotope record with a newly produced 1 Myr stack for Pacific Deep Water (PDW_{stack}) reveals that the intermediate depth levels off northern Chile were bathed by nearly pure PDW in past peak interglacial periods. This situation is in contrast to the modern hydrography that allows for some 30–40% contribution of AAIW to the water column properties at site GeoB15016. During cold phases of past interglacials and during glacial times, positive anomalies in the benthic $\delta^{13}C$ gradient ($\Delta\delta^{13}C$) between our intermediate record and the PDW_{stack} indicate that AAIW regularly reached our core site. Based on modern sea water $\delta^{13}C_{DIC}$ depth profiles, we demonstrate that glacial boundary conditions, i.e., lower sea level and a possible northward migration of the convection center of the AAIW associated with latitudinal migrations of the circum-Antarctic frontal systems account for ~50% of the increased $\Delta\delta^{13}C$ values with respect to preceding interglacials. Thus, we suggest that increased production of this water mass and/or deeper convection during cold periods could account for the remaining difference between the PDW_{stack} and our intermediate record. We note that potential changes in the actual preformed isotopic signature of the AAIW in the past 970 kyr could play a role in the $\delta^{13}C$ variability but remain unconstrained. The difference between our $\delta^{13}C$ record and the PDW_{stack} is largest during the LGM suggesting that this period witnesses the strongest presence of the AAIW in the SE Pacific since 970 ka, while its production was not necessary stronger than today's. The present situation with such strong convection of AAIW under a warm climate appears exceptional and raises questions regarding the situation during the Holocene climate optimum and the mechanisms behind the formation of the AAIW today and in the past.

[48] **Acknowledgments.** We thank the captain, crew, and scientific shipboard party of the German R/V *Sonne* cruise SO-211. We would like to thank the MARUM Isotope Laboratory at the University of Bremen, M. Segl and B. Meyer-Sack, as well as T. Westerhold, V. Lükies, and U. Röhl of MARUM, University of Bremen, Germany, for the support during the XRF measurements. T. Westerhold and A. Mix provided invaluable advice for generating the composite of the two drill cores. A. Mix furthermore shared useful discussions on the data interpretation. J. Castalino, A. Kramer, M. Zubrowski, and K. Grumbt are thanked for lab assistance. S. Roman, A. Mackensen, and R. Szarek provided useful insights in the benthic foraminiferal taxonomy. We thank M.J. Ruiz-Chancho, and A. Govin for help with the ANOVA tests. K. Kohlfeld and R. Graham generously shared a compilation on frontal movements in the Southern Ocean and M. Marchant unpublished benthic data of the Chilean margin. Special thanks go to M. Thierens for countless discussions. The GeoB and IODP core repositories in Bremen are thanked for sample storage and V. Bender, A. Wülbers, and W. Hale for support during sampling. G. Martínez-Méndez is funded through DFG-Research Center/Excellence Cluster "The Ocean in the Earth System" (MARUM fellowship). The ChiMeBo project is funded by the Bundesministerium für Bildung & Forschung (BMBF). R. De Pol-Holz received funding from Fondecyt grant 11100281 and FONDAP 15110009. H. Bostock is thanked for sharing information about seawater $\delta^{13}C$ in the Pacific and for her constructive review of our manuscript. Special thanks go to C. Charles (Editor) who provided his own expertise in a second review. The manuscript has been considerably improved through the revision process.

References

Anderson, R. F., S. Ali, L. I. Bradtmiller, S. H. H. Nielsen, M. Q. Fleisher, B. E. Anderson, and L. H. Burckle (2009), Wind-driven upwelling in the Southern Ocean and the deglacial rise in atmospheric CO_2, *Science*, *323*, 1443–1448.

Antonov, J. I., T. P. Seidov, T. P. Boyer, R. A. Locarnini, A. V. Mishonovov, H. E. Garcia, O. K. Baranova, M. M. Zweng, and D. R. Johnson (2010), *World Ocean Atlas 2009, Vol. 2: Salinity*, edited by S. Levitus, NOAA Atlas NESDIS 69, 184 pp., U.S. Government Printing Office, Washington. D. C.

Basak, C., E. E. Martin, K. Horikawa, and T. M. Marchitto (2010), Southern Ocean source of ^{14}C-depleted carbon in the North Pacific Ocean during the last deglaciation, *Nat. Geosci.*, *3*, 770–773.

Becquey, S., and R. Gersonde (2003), A 0.55-Ma paleotemperatre record from the Subantarctic zone: Implications for Antarctic Circumpolar Current development, *Paleoceanography*, *18*(1), 1014, doi:10.1029/2000PA000576.

Berger, W. H., K. Fisher, C. Lai, and G. Wu (1987), Ocean productivity and organic carbon flux. Part I. Overview and maps of primary production and export productivity, University of California, San Diego. SIO Reference 87–30, 67 pp.

Bostock, H. C., B. N. Opdyke, M. K. Gagan, and L. K. Fifield (2004), Carbon isotope evidence for changes in Antarctic Intermediate Water circulation and ocean ventilation in the southwest Pacific during the last deglaciation, *Paleoceanography*, *19*, PA4013, doi:10.1029/2004PA001047.

Bostock, H. C., P. J. Sutton, M. J. M. Williams, and B. N. Opdyke (2013), Reviewing the circulation and mixing of Antarctic Intermediate Water in the South Pacific using evidence from geochemical tracers and Argo float trajectories, *Deep Sea Res. Oceange. Res. Paper.*, *73*, 84–98.

Caniupán, M., et al. (2011), Millennial-scale sea surface temperature and Patagonian Ice Sheet changes off southernmost Chile (53°S) over the past ~60 kyr, *Paleoceanography*, *26*, PA3221, doi:10.1029/2010PA002049.

Charles, C. D., J. D. Wright, and R. G. Fairbanks (1993), Thermodynamic influences on the marine carbon isotope record, *Paleoceanography*, *8*, 691–697.

Curry, W. B., J. C. Duplessy, L. D. Labeyrie, and N. J. Shackleton (1988), Changes in the distribution of $\delta^{13}C$ of deep water CO_2 between the last glaciation and the Holocene, *Paleoceanography*, *3*(3), 317–341.

De Pol-Holz, R., L. Keigwin, J. Southon, D. Hebbeln, and M. Mohtadi (2010), No signature of abyssal carbon in intermediate waters off Chile during deglaciation, *Nat. Geosci.*, *3*, 192–195.

Dickson, B., J. Hurrell, N. Bindoff, A. Wong, B. Arbic, B. Owens, S. Imawaki, and I. Yashayaev (2001), Chapter 7.3. The world during WOCE, in *Ocean Circulation and Climate-Observing and Modelling the Global Ocean*, edited by G. Siedler, J. Church, and J. Gould, pp. 557–583, Academic Press, San Diego.

Duplessy, J. C., N. J. Shackleton, R. G. Fairbanks, L. Labeyrie, D. Oppo, and N. Kallel (1988), Deepwater source variations during the last climatic cycle and their impact on the global deepwater circulation, *Paleoceanography*, *3*(3), 343–360.

Elderfield, H., P. Ferretti, M. Greaves, S. Crowhurst, I. N. McCave, D. Hodell, and A. M. Piotrowski (2012), Evolution of ocean temperature and ice volume through the Mid-Pleistocene climate transition, *Science*, *337*, 704–709.

Fischer, H., et al. (2010), The role of Southern Ocean processes in orbital and millennial CO_2 variations—A synthesis, *Quaternary Sci. Rev.*, *29*(1–2), 193–205.

Flower, B. P., and J. P. Kennett (1995), Middle Miocene deepwater paleoceanography in the southwest Pacific: Relations with East Antarctic Ice Sheet development, *Paleoceanography*, *10*(6), 1095–1112.

Freudenthal, T., and G. Wefer (2007), Scientific drilling with the sea floor drill rig MeBo, *Sci. Drill.*, *5*, 63–66, doi:10.2204/iodp.sd.5.11.2007.

Freudenthal, T., and G. Wefer (2009), Shallow drilling in the deep sea: The sea floor drill rig MeBo, *Oceans '09 IEEE Bremen, IEEE Catalog Number: CFP09OCF-CDR*, *ISBN*: 978-1-4244-2523-5.

Gersonde, R., X. Crosta, A. Abelmann, and L. Armand (2005), Sea-surface temperature and sea ice distribution of the Southern Ocean at the EPILOG Last Glacial Maximum—A circum-Antarctic view based on siliceous microfossil records, *Quaternary Sci. Rev.*, *24*(7–9), 869–896.

Hanawa, K., and L. D. Talley (2001), Chapter 5.4. Mode waters, in *Ocean Circulation and Climate-Observing and Modelling the Global Ocean*, edited by G. Siedler, J. Church, and J. Gould, pp. 373–386, Academic Press, San Diego.

Hayward, B. W., A. T. Sabaa, A. Kolodziej, M. P. Crundwell, S. Steph, G. H. Scott, H. L. Neil, H. C. Bostock, L. Carter, and H. R. Grenfell (2012), Planktic foraminifera-based sea-surface temperature record in the Tasman Sea and history of the Subtropical Front around New Zealand, over the last one million years, *Mar. Micropaleo.*, *82–83*(0), 13–27.

Hebbeln, D., F. Lamy, M. Mohtadi, and H. Echtler (2007), Tracing the impact of glacial-interglacial climate variability on erosion of the southern Andes, *Geology*, *35*, 131–134.

Herguera, J. C., T. D. Herbert, M. Kashgarian, and C. Charles (2010), Intermediate and deep water mass distribution in the Pacific during the Last Glacial Maximum inferred from oxygen and carbon stable isotopes, *Quaternary Sci. Rev.*, *19*, 1228–1245.

Ho, S. L., G. Mollenhauer, F. Lamy, A. Martínez-Garcia, M. Mohtadi, R. Gersonde, D. Hebbeln, S. Nuñez-Ricardo, A. Rosell-Melé, and R. Tiedemann (2012), Sea surface temperature variability in the Pacific sector of the Southern Ocean over the past 700 kyr, *Paleoceanography*, *27*, PA4202, doi:10.1029/2012PA002317.

Hodell, D. A., C. D. Charles, and F. J. Sierro (2001), Late Pleistocene evolution of the ocean's carbonate system, *Earth Planet. Sci. Lett.*, *192*(2), 109–124.

Hodell, D. A., K. Venz, C. D. Charles, and U. S. Ninnemann (2003), Pleistocene vertical carbon isotope and carbonate gradients in the South Atlantic sector of the Southern Ocean, *Geochem. Geophys. Geosys.*, *4*(1), 1004, doi:10.1029/2002GC000367.

Holbourn, A., W. Kuhnt, J. A. Simo, and Q. Li (2004), Middle Miocene isotope stratigraphy and paleoceanographic evolution of the northwest and southwest Australian margins (Wombat Plateau and Great Australian Bight), *Palaeogeogr. Palaeoclim. Palaeoecol.*, *208*(1–2), 1–22.

Hoogakker, B. A. A., E. J. Rohling, M. R. Palmer, T. Tyrrell, and R. G. Rothwell (2006), Underlying causes for long-term global ocean $\delta^{13}C$ fluctuations over the last 1.20 Myr, *Earth Planet. Sci. Lett.*, *248*(1–2), 15.

Keeling, R. F., and B. B. Stephens (2001), Antarctic sea ice and the control of plesitocene climate instability, *Paleoceanography*, *16*(1), 112–131.

Keigwin, L. D. (1987), North Pacific deep water formation during the latest glaciation, *Nature*, *330*, 362–364.

Kohfeld, K. E., R. M. Graham, A. M. de Boer, L. C. Sime, E. W. Wolff, C. Le Quéré, and L. Bopp (2013), Southern Hemisphere westerly wind changes during the Last Glacial Maximum: Paleo-data synthesis, *Quaternary Sci. Rev.*, *68*, 76–95.

Kroopnick, P. M. (1985), The distribution of ^{13}C of ΣCO_2 in the world oceans, *Deep Sea Res. Oceanogr. Res. Paper.*, *32*(1), 57–84.

Kumamoto, Y., A. Murata, S. Watanabe, and M. Fukasawa (2011), Temporal and spatial variations in bomb-produced radiocarbon along BEAGLE2003 lines—Revisits of WHP P06, A10, and I03/I04 in the Southern Hemisphere Oceans, *Prog. Oceanogr.*, *89*(1–4), 49–60.

Leth, O., G. Shaffer, and O. Ulloa (2004), Hydrography of the eastern South Pacific Ocean: Results from the *Sonne* 102 cruise, May–June 1995, *Deep Sea Res. Topical Stud. Oceanogr.*, *51*(20–21), 2349–2369.

Lisiecki, L. E. (2010), A simple mixing explanation for late Pleistocene changes in the Pacific-South Atlantic benthic $\delta^{13}C$ gradient, *Clim. Past*, *6*, 305–314.

Lisiecki, L. E., and M. E. Raymo (2005), A Pliocene-Pleistocene stack of 57 globally distributed benthic $\delta^{18}O$ records, *Paleoceanography*, *20*, PA1003, doi:10.1029/2004PA001071.

Llanillo, P. J., J. L. Pelegrí, C. M. Duarte, M. Emelianov, M. Gasser, J. Gourrion, and A. Rodríguez-Santana (2012), Meridional and zonal changes in water properties along the continental slope off central and northern Chile, *Cienc. Mar.*, *38*(1B), 307–332.

Mackensen, A., H. W. Hubberten, T. Bickert, G. Fischer, and D. K. Fütterer (1993), The $\delta^{13}C$ in benthic foraminiferal tests on *Fontbotia wuellerstorfi* (Schwager) relative to the $\delta^{13}C$ of dissolved inorganic carbon in southern ocean deep water: Implications for glacial ocean circulation models, *Paleoceanography*, *8*(5), 587–610.

Makou, M. C., D. W. Oppo, and W. B. Curry (2010), South Atlantic intermediate water mass geometry for the last glacial maximum from foraminiferal Cd/Ca, *Paleoceanography*, *25*, PA4101, doi:10.1029/2010PA001962.

Marchitto, T. M., J. L. Scott, J. D. Ortiz, J. Flückiger, and A. van Geen (2007), Marine radiocarbon evidence for the mechanism of deglacial atmospheric CO_2 rise, *Science*, *316*, 1456–1461.

McCartney, M. (1977), Subantarctic mode water, in *A Voyage of Discovery*, edited by M. Angel, pp. 103–119, Pergamon Press, London.

Mohtadi, M., D. Hebbeln, S. Nuñez Ricardo, and C. B. Lange (2006), El Niño-like pattern in the Pacific during marine isotope stages (MIS) 13 and 11?, *Paleoceanography*, *21*, PA1015, doi:10.1029/2005PA001190.

Mohtadi, M., P. Rossel, C. B. Lange, S. Pantoja, P. Böning, D. J. Repeta, M. Grunwald, F. Lamy, D. Hebbeln, and H.-J. Brumsack (2008), Deglacial pattern of circulation and marine productivity in the upwelling region off central-south Chile, *Earth Planet. Sci. Lett.*, *272*(1–2), 221–230.

Molinelli, E. T. (1981), The Antarctic influence on Antractic Intermediate Water, *J. Mar. Res.*, *39*, 267–293.

Mook, W. G., J. C. Bommerson, and W. H. Stoverman (1974), Carbon isotope fractionation between dissolved bicarbonate and gaseous carbon dioxide, *Earth Planet. Sci. Lett.*, *22*, 69–176.

Muratli, J. M., Z. Chase, A. C. Mix, and J. McManus (2010), Increased glacial-age ventilation of the Chilean margin by Antarctic Intermediate Water, *Nat. Geosci.*, *3*(1), 23–26.

Pahnke, K., and R. Zahn (2005), Southern Hemisphere water mass conversion linked with North Atlantic climate variability, *Science*, *307*, 1,741–741,746.

Pahnke, K., S. L. Goldstein, and S. R. Hemming (2008), Abrupt changes in Antarctic Intermediate Water circulation over the past 25,000 years, *Nat. Geosci.*, *1*, 870–874.

Rintoul, S. R. (1991), South Atlantic interbasin exchange, *J. Geophys. Res.*, *96*, 2675–2692.

Röhl, U., and L. J. Abrams (2000), High-resolution, down-hole and non-destructive core measurements from Sites 999 and 1001 in the Caribbean Sea: Application to the Late Paleocene Thermal Maximum, *Proceedings of the Ocean Drilling Program (ODP), Scientific Results 165*, 191–203, College Station, TX (Ocean Drilling Program).

Romero, O. E., J.-H. Kim, and D. Hebbeln (2006), Paleoproductivity evolution off central Chile from the Last Glacial Maximum to the Early Holocene, *Quaternary Res.*, *65*(3), 519–525.

Rose, K. A., E. L. Sikes, T. P. Guilderson, P. Shane, T. M. Hill, R. Zahn, and H. J. Spero (2010), Upper-ocean-to-atmosphere radiocarbon offsets imply fast deglacial carbon dioxide release, *Nature*, *466*, 1093–1097.

Sabine, C. L., et al. (2004), The oceanic sink for Anthropogenic CO_2, *Science*, *305*, 367–371.

Saenko, O. A., A. J. Weaver, and J. M. Gregory (2003), On the link between the two modes of the ocean thermohaline circulation and the formation of global-scale water masses, *J. Climate*, *16*(17), 2,797–792,801.

Sallee, J.-B., R. J. Matear, S. R. Rintoul, and A. Lenton (2012), Localized subduction of anthropogenic carbon dioxide in the Southern Hemisphere oceans, *Nat. Geosci.*, *5*(8), 579–584.

Schäfer, G., J. S. Rodger, B. W. Hayward, J. P. Kennett, A. T. Sabaa, and G. H. Scott (2005), Planktic foraminiferal and sea surface temperature record during the last 1 Myr across the Subtropical Front, Southwest Pacific, *Mar. Micropaleo.*, *54*(3–4), 191.

Schlitzer, R. (2012), Ocean Data View, http://odv.awi.de.

Schmidtko, S., and G. C. Johnson (2012), Multidecadal warming and shoaling of Antarctic Intermediate Water, *J. Climate*, *25*, 207–221.

Schneider, W., R. Fuenzalida, R. Nuñez, L. Bravo, and D. Figueroa (2007), Discussion of the Humboldt Current System and water masses in the North and Center off Chile, *Cienc. Tecnol. Mar*, *301*, 21–36.

Shaffer, G., S. Hormazabal, O. Pizarro, and M. Ramos (2004), Circulation and variability in the Chile Basin, *Deep Sea Res.. Oceanogr. Res. Paper*, *51*(10), 1367–1386.

Sijp, W. P., and M. H. England (2009), Southern Hemisphere westerly wind control over the ocean's thermohaline circulation, *J. Climate*, *22*, 1277–1286.

Silva, N., N. Rojas, and A. Fedele (2009), Water masses in the Humboldt Current System: Properties, distribution, and the nitrate deficit as a chemical water mass tracer for Equatorial Subsurface Water off Chile, *Deep Sea Res. Topical Stud. Oceanogr.*, *56*(16), 1004–1020.

Sloyan, B. M., and S. R. Rintoul (2001), Circulation, renewal, and modification of Antarctic Mode and Intermediate Water, *J. Phys. Oceanogr.*, *31*(4), 1005–1030.

Sortor, R. N., and D. C. Lund (2011), No evidence for a deglacial intermediate water $\Delta^{14}C$ anomaly in the SW Atlantic, *Earth Planet. Sci. Lett.*, *310*(1–2), 65–72.

Talley, L. D. (1999), Some aspects of ocean heat transport by the shallow, intermediate and deep overturning circulations, in *Mechanisms of Global Climate Change at Millennial Time Scales*, *Geophys. Monogr. Ser.*, vol. 112, edited by U. Clark, S. Webb, and D. Keigwin, pp. 1–22, AGU, Washington, D. C., doi:10.1029/GM112p0001.

Talley, L. (2005), WOCE P19 vertical sections, http://www.word.ucsd.edu/whp_atlas//pacific/p19/sections/printatlas/printatlas.htm, http://cchdo.ucsd.edu/cruise/316N145_14.

Wainer, I., M. Goes, L. N. Murphy, and E. Brady (2012), Changes in the intermediate water mass formation rates in the global ocean for the Last Glacial Maximum, mid-Holocene and pre-industrial climates, *Paleoceanography*, *27*, PA3101,doi:10.1029/2012PA002290.

Wong, A. P. S., N. L. Bindoff, and J. A. Church (1999), Large-scale freshening of intermediate waters in the Pacific and Indian oceans, *Nature*, *400*, 440–443.

Zahn, R., K. Winn, and M. Sarnthein (1986), Benthic foraminiferal $\delta^{13}C$ and accumulation of organic carbon: *Uvigerina perigerina* and *Cibicidoides wuellerstorfi*, *Paleoceanography*, *1*(1), 27–42.